Received: 6 February 2021 | Revised: 7 April 2021 | Accepted: 26 April 2021

DOI: 10.1002/cyto.a.24361

BRIEF REPORT

MIFlowCyt

ISAC CYTOMETRY Journal of Quantitative Cell Science PART A

Sheath fluid impacts the depletion of cellular metabolites in cells afflicted by sorting induced cellular stress (SICS)

Kamilah Ryan[1] | Rebecca E. Rose[2] | Drew R. Jones[2] | Peter A. Lopez[1]

[1]Cytometry and Cell Sorting Laboratory, NYU Langone Health, New York City, New York, USA

[2]Metabolomics Core Resource Laboratory, NYU Langone Health, New York City, New York, USA

Correspondence
Peter A. Lopez, 540 First Ave, SK3 Lab 9, New York, NY 10016 USA.
Email: peter.lopez@nyulangone.org

Funding information
National Cancer Institute, Grant/Award Number: P30CA016087; National Institutes of Health, Grant/Award Numbers: HHS-NIH-NIAD-BAA2018, R01 NS108151-01, RFA 2018-PACT001; New York State Stem Cell Science, Grant/Award Number: C023058

Abstract

Flow cytometrists have long observed a spectrum of cell-type-specific changes ranging from minor functional defects to outright cell destruction after purification of cells using conventional droplet cell sorters. We have described this spectrum of cell perturbations as sorter induced cellular stress, or SICS (Lopez and Hulspas, Cytometry, 2020, 97, 105–106). Despite the potential impact of this issue and ubiquitous anecdotes, little has been reported about this phenomenon in the literature, and the underlying mechanism has been elusive. Inspired by others' observations (Llufrio et al., Redox Biology, 2018, 16, 381–387 and Binek et al., Journal of Proteome Research, 2019, 18, 169–181), we set out to examine SICS at the metabolic level and use this information to propose a working model. Using representative suspension (Jurkat) and adherent (NIH/3T3) cell lines we observed broad and consistent metabolic perturbations after sorting using a high-speed droplet cell sorter. Our results suggest that the SICS metabolic phenotype is a common cell-type-independent manifestation and may be the harbinger of a wide-range of functional defects either directly related to metabolism, or cell stress response pathways. We further demonstrate a proof of concept that a modification to the fluidic environment (complete media used as sheath fluid) in a droplet cell sorter can largely rescue the intracellular markers of SICS, and that this rescue is not due to a contribution of metabolites found in media. Future studies will focus on characterizing the potential electro-physical mechanisms inherent to the droplet cell sorting process to determine the major contributors to the SICS mechanism.

KEYWORDS
cell sorting, cytometry, FACS, metabolism, metabolomics, SICS

1 | INTRODUCTION

Since the realization of cell purification by electrostatic droplet sorters [1,2], users of this technology have anecdotally observed that certain types of cells are especially sensitive to the sorting process and can be rendered non-viable, or even destroyed, under typical sorting conditions. Conventional droplet sorters all impart similar forces that could be disruptive to living cells. Many factors inherent to the conventional cell sorting process have been considered as potential contributors to SICS, including sheer force (function of nozzle orifice diameter), rapid pressure changes (pressurization and depressurization), rapid acceleration and deceleration (nozzle and collection receptacle), the varied polarity high voltage charge applied to the stream for droplet deflection, temperature changes, buffer chemistry, and the

Kamilah Ryan and Rebecca E. Rose contributed equally to this study.

overall impact of removing cells from their homeostatic environment in the tissue culture incubator [3-7].

Sorter induced cellular stress (SICS) encompasses all cellular changes caused specifically by the cell sorting process and can manifest in many ways. While previous studies have shown limited impact on gene expression due to cell sorting [8-10], functional changes have been reported in cells after cell sorting, including p38 MAPK activation in T-cells [3,11], diminished antigen presentation by dendritic cells [4], and arrested growth in T-cell subsets cultured immediately after sorting (personal communication, Alan Saluk). In the case of some cell types, such as cardiomyocytes or neuronal cells, sorting with a conventional droplet cell sorter is rarely successful due to poor cell viability post-sort. While ad hoc and cell-type-specific techniques have been devised [12] to minimize SICS, these efforts have not identified an underlying mechanism or provide a universal approach to mitigate these effects. General best practices in flow cytometry have been proposed (e.g., temperature control, lower system pressure, larger nozzle orifice, etc.) but these commonsense measures do not eliminate SICS across all cell types, or necessarily rescue the functional deficits [6]. Several cell types including the DI TNC1 rat astrocytic cell line and primary murine peritoneal macrophages have also been reported to be unreliable for downstream metabolomic assays after purification by cell sorting [13,14]. We have noted similar post-sorting metabolomic perturbations using Jurkat, NIH/3T3, and various immune cell types (data not shown) with severe depletion of most cellular metabolites after cell sorting. We chose to focus on the metabolic manifestation of SICS instead of cell-type-specific functional changes in order to better understand the cell sorter's contribution to SICS. We hypothesized that the metabolic profile might show signatures of these effects due to the transient nature of sorting, and the time-sensitivity of metabolism. The fact that the depleted metabolomic profile post-sort is not limited to specific cell types led us to focus on metabolic SICS markers and this approach will enable further studies into the myriad potentially disruptive factors at play in the cell sorting process.

2 | EXPERIMENTAL RATIONALE AND DESIGN

We aimed to test two overarching potential explanations for SICS; that cells are outside of homeostatic conditions due to sorting or that the physical forces involved in the cytometer's sorting process impact cellular integrity. Due to the complexity of potential factors involved, we designed a proof-of-concept study with a simple intervention to begin testing these hypotheses. Our choice to initially focus on sheath fluid composition was inspired by an observation from the use of counterflow centrifugal elutriation (personal communication, Peter A. Lopez), a label-free and gentle cell purification process [15]. CCE exposes cells to an elutriation buffer used to carry purified cell types out of a centrifuge rotor for collection. Previous studies in our lab (data not shown) found that cells purified by CCE for use in a metabolomics assay exhibited depletion of metabolites when using PBS as the elutriation buffer. This was mitigated in our lab by using complete media as the elutriation buffer in place of PBS. With this observation in mind, we chose to test if complete media used as sheath fluid might rescue metabolomic SICS in droplet-sorted cells. Since metabolic processes are extremely state and time-dependent, our study benefited from the availability of the Sony SY3200 dual-head parallel cell sorter, which allows two simultaneous but independent cell sorts to occur within the same instrument. Using this cell sorter, we were able to expose aliquots of the same starting population in a pairwise fashion to different experimental conditions while controlling for almost all experimental artifacts between the two conditions; including the time out of incubator, temperature, instrumentation, instrument operational parameters, sample processing, and so forth. This cell sorter, which employs the same electrostatic droplet cell sorting operational parameters common to all conventional droplet sorters [1], controls for the variable of timing that would be introduced if these experiments were performed serially on one cell sorter.

Adherent (NIH/3T3) and non-adherent (Jurkat) cell lines were used to confirm previous observations [13,14] of post-sort metabolic perturbation, as well as to evaluate the potential mitigation of the metabolic SICS phenotype afforded by replacing standard electrolyte-containing sheath fluid with complete media. Unlabeled cells were suspended in complete media and identical aliquots of 1 ml were prepared for unsorted controls as well as for pairwise sorting using the SY3200 (Figure 1). Technical replicate control aliquots ($n = 3$) were spun down and flash frozen at the start of each sorting experiment to represent the "ideal" pre-sorted cell population ($Control_{start}$). Cells were sorted from within a region drawn on a forward scatter versus side scatter plot (Figure 1Ai,Aii) that excluded small debris and aggregates. Aliquots of the same unlabeled samples were sorted simultaneously on HAPS 1 and 2 using different combinations of sheath and collection fluids. Single-way sorts were performed ($n = 3$) in parallel to produce replicate sorted samples for each sheath/collection fluid combination, for example, $Sheath_{PBS}$ $Collect_{RPMI}$ (Figure 1C,D). Directly comparable parallel sorts are indicated by line type (dashed or solid) which do not illustrate a two-way sort or the sort direction. Replicate control aliquots ($n = 3$) were either kept in the incubator or at room temperature for the duration of sorting (Figure 1E). For harvesting, sorted and unsorted control samples were centrifuged at 1000*g* for 3 min at 25°C. Supernatant was aspirated and discarded leaving 1 ml. The cell pellets were resuspended in 1 ml of PBS and transferred into 1.5 ml Eppendorf tubes (Fisherbrand, 02-681-5) and centrifuged a second time at 1000 g and 25°C for 3 min. All supernatant was aspirated and discarded, leaving behind only the cell pellet, which was placed on dry ice and then into −80°C storage until metabolomic processing.

3 | MATERIALS AND METHODS

3.1 | Cell culture

Jurkat and NIH/3T3 cells were each cultured in RPMI 1640 medium (HyClone, SH30027.01), with the addition of 10% fetal bovine serum (Corning, 35-011-CV), 1.0% penicillin/streptomycin (Gibco, 15140122), and 1.5% HEPES buffer (Gibco, 15630-080). In addition

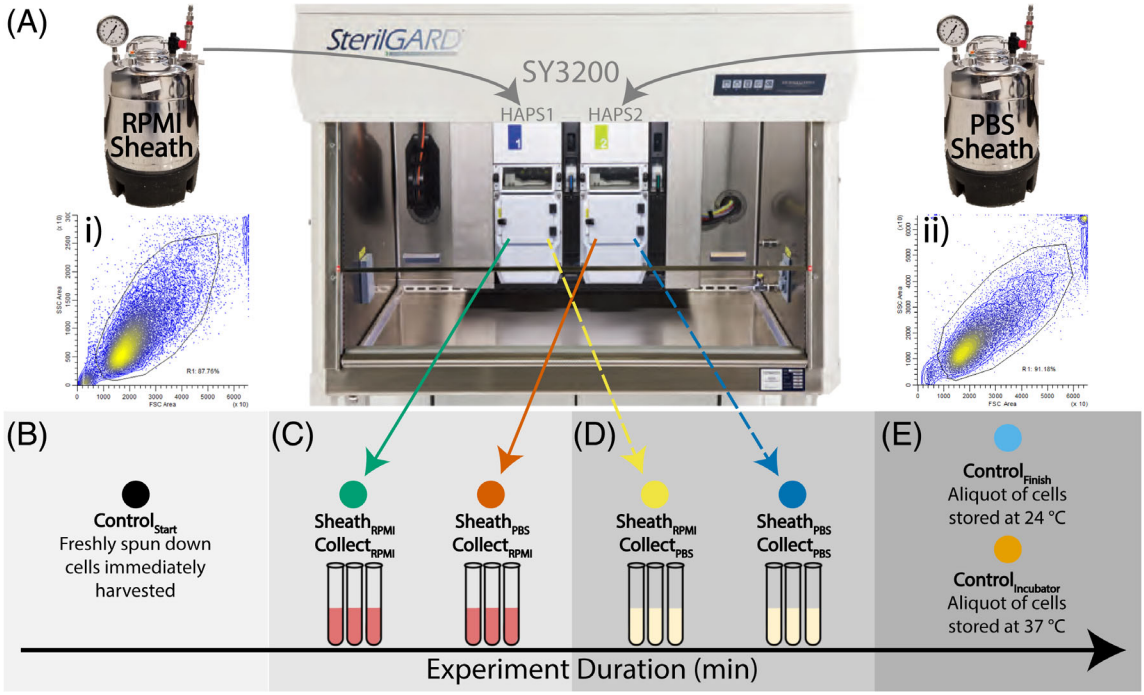

FIGURE 1 Overall experimental workflow—Pairwise sorting and unsorted controls cultured cells were aliquoted into control conditions (B and E) and various sorted conditions (C and D). Sorting was carried out in a pairwise fashion (indicated by solid or dashed arrows) on the SY3200. Control and sorted cells were pelleted, frozen, and analyzed by LC–MS/MS. Colored dots indicate experimental groups:
Black – $Control_{Start}$, unsorted cells pelleted at the start of th e experiment
Sky Blue – $Control_{Finish}$, unsorted cells kept at RT for experiment duration and pelleted at the end ofthe experiment
Orange– $Control_{Incubator}$, unsorted cells kept in incubator for the duration of the experiment
Blue– $Sheath_{PBS}$ $Collect_{PBS}$, sorted cells with sheath fluid of PBS and collectionfluid of PBS
Vermillion – $Sheath_{PBS}$ $Collect_{RPMI}$, sorted cells with sheath fluid of PBS collection fluid of RPMI
Yellow – $Sheath_{RPMI}$ $Collect_{PBS}$, sorted cells with sheath fluid of RPMI collection fluidof PBS
Green – $Sheath_{RPMI}$ $Collect_{RPMI}$, sorted cells with sheath fluid of RPMI and collectionfluid of RPMI

of supplements media was sterile filtered (Nalgene rapid-flow 75 mm filter unit, 0.2 μm, 500 ml, Thermo Scientific, 566-0020). Cells were cultured in a 5% CO_2 incubator at 37°C and were grown in T75 culture flasks (Falcon, 1368065) containing 15–20 ml of media. Cells were allowed to grow and acclimate in culture for 2–3 weeks before use and were split at either 1:10 or 1:20 at 3-day intervals. Cells were harvested for each cell sorting experiment 3–4 days after splitting. Jurkat cells were aspirated from the culture flask before sorting, while NIH/3T3 cells were removed from culture by first aspirating all media from the flask, washing the cell lawn with 10 ml Dulbecco's phosphate-buffered saline (DPBS, Gibco, 14190-144), detachment from the plate by trypsinization using 3 ml of trypsin for 3 min at 37°C, followed by the addition of 10 ml complete RPMI media. Cells were removed after repeated pipetting and aspirated. After removal from tissue culture, Jurkat and NIH/3T3 cells were centrifuged at 300*g* for 5 min at 25°C. Cells were resuspended in 1 ml of RPMI media for counting and viability determination using a Cellometer Auto 2000 cell counter (Nexcelom). All cell samples showed >90% viability and were strained through a 50 μm cell strainer (Sysmex CellTrics, 04–004202317) then divided into two equal aliquots containing 1–2 × 10^7 cells for sorting. Cells were not labeled or further processed before cell sorting.

3.2 | Cell sorting and unsorted controls

Two aliquots of the same starting population were sorted simultaneously using a Sony SY3200 dual-headed parallel cell sorter. Each highly automated parallel sorter (HAPS) module contained within the SY3200 sorter was configured with a different sheath fluid for pairwise comparison. HAPS1 was outfitted with the same formulation of RPMI 1640 described earlier for tissue culture, while HAPS2 used modified Dulbecco's phosphate buffer (mDPBS: 80 g sodium chloride, 2 g potassium chloride, 14.4 g disodium phosphate, and 2.4 monopotassium phosphates per liter of distilled water, NYULH Research Support Service) as sheath fluid. All sheath fluids were used at room temperature and sterile filtered (0.2 μm filter) before use. In-line sheath filters were removed from each HAPS to minimize carryover of sheath fluids. Each HAPS was configured with a 100 μm nozzle and was operated under similar operating conditions. Sheath pressure was 25 psi on both HAPS 1 and 2 with a drop drive frequency of 32.3 and 32.8 kHz on HAPS1 and 2, respectively. While HAPS1 and HAPS2 are physically identical sorters operating within the same enclosure they operate as independent cell sorters and, as such, may have slightly different instrument operational settings and data appearance. Cells were sorted on each HAPS in a single-way sort at a total event rate of

8000–10,0000 events per second at room temperature, and 1 million cells were sorted into collection tubes (Falcon 352063) containing 1 ml of either RPMI or mDPBS as collection fluid.

3.3 | Metabolite extraction and LC–MS/MS analysis

Samples were subjected to an LCMS analysis to detect and quantify known peaks. A metabolite extraction was carried out on each sample with a previously described method [16]. The LC column was a Millipore™ ZIC-pHILIC (2.1 × 150 mm, 5 μm) coupled to a Dionex Ultimate 3000™ system and the column oven temperature was set to 25°C for the gradient elution. A flow rate of 100 μl/min was used with the following buffers; (A) 10 mM ammonium carbonate in water, pH 9.0, and (B) neat acetonitrile. The gradient profile was as follows: 80%–20%B (0–30 min), 20%–80%B (30–31 min), 80%–80%B (31–42 min). Injection volume was set to 2 μl for all analyses (42 min total run time per injection). MS analyses were carried out by coupling the LC system to a Thermo Q Exactive HF™ mass spectrometer operating in heated electrospray ionization mode (HESI). Method duration was 30 minutes with a polarity switching data-dependent Top five method for both positive and negative modes. Spray voltage for both positive and negative modes was 3.5 kV and the capillary temperature was set to 320°C with a sheath gas rate of 35, aux gas of 10, and max spray current of 100 μA. The full MS scan for both polarities utilized 120,000 resolution with an AGC target of 3e6 and a maximum IT of 100 ms, and the scan range was from 67 to 1000 m/z. Tandem MS spectra for both positive and negative mode used a resolution of 15,000, AGC target of 1e5, maximum IT of 50 ms, isolation window of 0.4 m/z, isolation offset of 0.1 m/z, fixed first mass of 50 m/z, and three-way multiplexed normalized collision energies (nCE) of 10, 35, 80. The minimum AGC target was 1e4 with an intensity threshold of 2e5. All data were acquired in profile mode.

3.4 | Metabolomics data processing

The resulting Thermo™ RAW files with ThermoFisher CommonCore RawFileReader, and an in-house python script (Skeleton) was used for peak detection and quantification of all internal standards and sample peaks based on a previously established library of metabolite retention times and accurate masses adapted from the Whitehead Institute [14], and verified with authentic standards and/or high-resolution MS/MS spectra manually curated against the NIST14 MS/MS [17] and METLIN (2017) [18] tandem mass spectral libraries. Annotation coverage was expanded by searching all data-dependent MS/MS spectra against the NIST and METLIN spectral libraries. Metabolites scoring higher than RevDot 900 were retained for relative quantification. Untargeted features were further assessed with an in-house python script (Ungrid) which was used to detect all representative MS1 peaks across the samples using an *m/z* discrimination threshold of 20 ppm, a minimum peak intensity of 1e5 for the representative peak, a minimum signal-to-noise ratio of 10, and a retention time discrimination threshold of 2 min. Known metabolites, putative metabolites, and metabolite features were then extracted based on either the detected *m/z* of the feature or the theoretical *m/z* of the expected ion type for the known or matched standard metabolite in the library (e. comparisons, and *t* tests were performed with the Python SciPy (1.1.0) [19] library to test for differences and generate statistics for downstream g., $[M + H]^+$), and prioritized by this rank order. Tolerances for peak quantification were ± 7.5 part-per-million (ppm) mass accuracy, ± 7.5 s peak apex retention time tolerance within an initial retention time search window of ±0.5 min across the study samples. Redundant putative metabolites and features were removed using the sum peak intensity of all samples for a given row and retaining the highest priority annotation. The resulting data matrix of metabolite intensities for all samples and blank controls was processed with an in-house statistical pipeline, Metabolyze Github commit 765770e, and final detection was calculated based on a signal-to-noise ratio (S/N) of 3X compared with blank controls, with a floor of 10,000 (arbitrary units). For samples where the peak intensity was lower than the blank threshold, metabolites or features were annotated as not detected, and the threshold value was imputed for any statistical comparisons to enable an estimate of the fold change and *p*-value as applicable. This blank corrected data matrix was then used for all group-wise analyses. Any metabolite with *p*-value <0.05 was considered significantly regulated (up or down), unless otherwise specified. Heatmaps were generated with hierarchical clustering performed on the imputed matrix values utilizing the R library, pheatmap (1.0.12) [20]. Volcano plots were generated utilizing the R library, Manhattanly (0.2.0). Pathway analyses were carried out manually using Metaboanalyst 5.0 on the website. Matched names were checked manually, and pathway analysis parameters used the hypergeometric test, relative-betweenness centrality, and all compounds in the selected pathway library for the reference metabolome with the *Homo sapiens* KEGG database. www.metaboanalyst.ca website. Matched names were checked manually, and pathway analysis parameters used the hypergeometric test, relative-betweenness centrality, and all compounds in the selected pathway library for the reference metabolome with the *Homo sapiens* KEGG database.

4 | RESULTS

4.1 | Global metabolomics assessment of SICS

We carried out a global/untargeted metabolomics analysis to provide an un-biased assessment of the scope and breadth of the SICS metabolic phenotype. We also evaluated an adherent cell line (NIH/3T3 cells) to determine if the SICS phenomenon is affected by cellular adhesion and again used the parallel sorter to directly compare various sorting conditions. Overall, we acquired relative quantification on 696 putatively identified or standard library metabolites, and 621 high-intensity/non-redundant untargeted metabolite features ($n = 1316$ total analytes) (Table S1). Based on the resulting principal

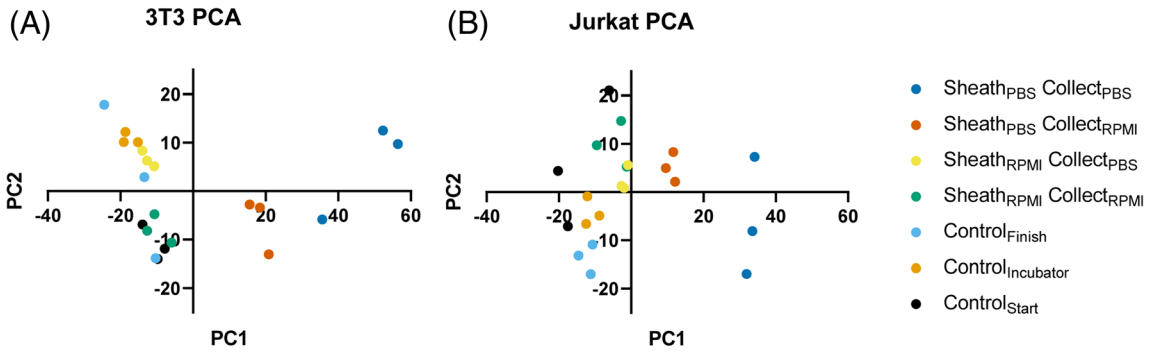

FIGURE 2 Metabolomics PCA model of SICS conditions principal components analysis of the metabolic profiles of an (A) adherent NIN/3T3 (3T3) and (B) nonadherent (Jurkat) cell. Each flow cytometry sort was carried out in technical triplicate. All replicates were derived from the same flask of cells

components model of the metabolic profile, the un-sorted Control$_{Start}$ (black) cells were found to cluster distantly and distinctly from the NIH/3T3 cells sorted using sheath fluid of PBS collected into PBS (Sheath$_{PBS}$ Collect$_{PBS}$, blue) (Figure 2A). Closer examination showed that this due to a large population ($n = 508$) of significantly downregulated ($p < 0.01$, >twofold) metabolites. (Figure S1A). Notably, a pathway analysis of this subset of metabolites suggests that *Arginine biosynthesis* (13/14 metabolites, Holm Adj p = 1.21e-8) and *Alanine, aspartate, and glutamate metabolism* (18/28 metabolites, Holm Adj p = 1.68 e-7) were the most impacted pathways (Table S3), though many diverse metabolite pathways were also impacted including nucleotides, TCA cycle, amino acids, pentose phosphate, and others. Only a small population ($n = 20$) of metabolites and metabolite features were significantly upregulated ($p < 0.01$, > twofold), and were identified as AMP, UMP, IMP, Phosphorylcholine, and Palmitoyl carnitine. The overall PCA model appeared similar when we applied the same conditions to the suspension Jurkat cells (Figure 2B). Coverage of the Jurkat profile was similar with 521 putatively identified or standard library metabolites, and 434 high-intensity/non-redundant untargeted metabolite features ($n = 954$ total analytes) (Table S2). Again, a broad ($n = 193$) downregulation ($p < 0.01$, > twofold) of metabolites was observed (Figure S1B), and a pathway analysis of this subset of metabolites also found *Arginine biosynthesis* (8/14 metabolites, Holm Adj p = 2.93e-6) being disproportionately found, along with other pathways especially related to amino acids (Table S4). Again, only a few Jurkat ($n = 5$) metabolites were significantly upregulated ($p < 0.01$, > twofold), consisting of Pipecolic acid, and several un-annotated features.

4.2 | Effect of collection fluid

We next considered the effect of collection fluid type on the apparent changes to the metabolic profile in a pairwise sort with the SY3200. We hypothesized that with Sheath$_{PBS}$, we could evaluate the impact of the post-sort cellular environment using different collection fluids (Collect$_{PBS}$ or Collect$_{RPMI}$). Qualitatively, the PCA model shows that Collect$_{RPMI}$ (vermillion and green dots) samples are shifted in the direction of Control$_{Start}$ cells (black dots) indicating that the metabolic profile is becoming more similar to Control$_{Start}$ samples. However, the Collect$_{RPMI}$ samples still clustered most closely with the highly depleted Sheath$_{PBS}$ Collect$_{PBS}$ condition (Figure 2A, blue dots). Collect$_{RPMI}$ led to an increase in almost all amino acids, and a fairly broad but modest recovery ($n = 137$) of many other metabolites ($p < 0.01$, >twofold). Only a few ($n = 7$) metabolites change the other direction ($p < 0.01$, >twofold) after Collect$_{RPMI}$, and this group overlapped with the metabolites that were upregulated in the previous Sheath$_{PBS}$ Collect$_{PBS}$ versus starting unsorted control populations described above (Figure S2). These metabolites were Cytidine, Uridine, UMP, IMP, AMP, Palmitoyl carnitine, and an untargeted feature "Feature_ + _219.1417_6.8," which was also upregulated in the previous comparison. Therefore, this feature was manually inspected, and annotated as a natural isotope of Propionyl carnitine (Main feature: $p = 0.002$, FC = 1.6-fold downregulated, Figure S3). This subset of metabolites could therefore represent key markers of cell stress caused by the cellular environment during post-sorting conditions, but not necessarily SICS since the media collection fluid only provides a partial rescue of the phenotype. These overall trends were recapitulated in the Jurkat study (Figure 2B), and Collect$_{RPMI}$ broadly rescued many metabolites ($n = 190$) and metabolite features ($p < 0.01$, >twofold). Only two metabolites were downregulated with the same criteria, and both were untargeted features (Feature_ + _168.0897_7.7, Feature_ + _172.0667_10.0). Interestingly, these features were also among the shortlist ($n = 5$) of metabolites that were upregulated in Sheath$_{PBS}$ Collect$_{PBS}$ versus Control$_{Start}$ cells discussed above.

4.3 | Effect of sheath fluid

Next, the effect of modifying the sheath fluid was assessed, while using Collect$_{PBS}$ for both sorts (pairwise). Compared with the Sheath$_{PBS}$ (blue dots), the cells sorted with Sheath$_{RPMI}$ (yellow dots) were distant and tightly clustered. The Sheath$_{RPMI}$ group was close to the Control$_{Incubator}$ samples which were un-sorted, indicating that Sheath$_{RPMI}$ makes the metabolic profile more like unsorted cells. The

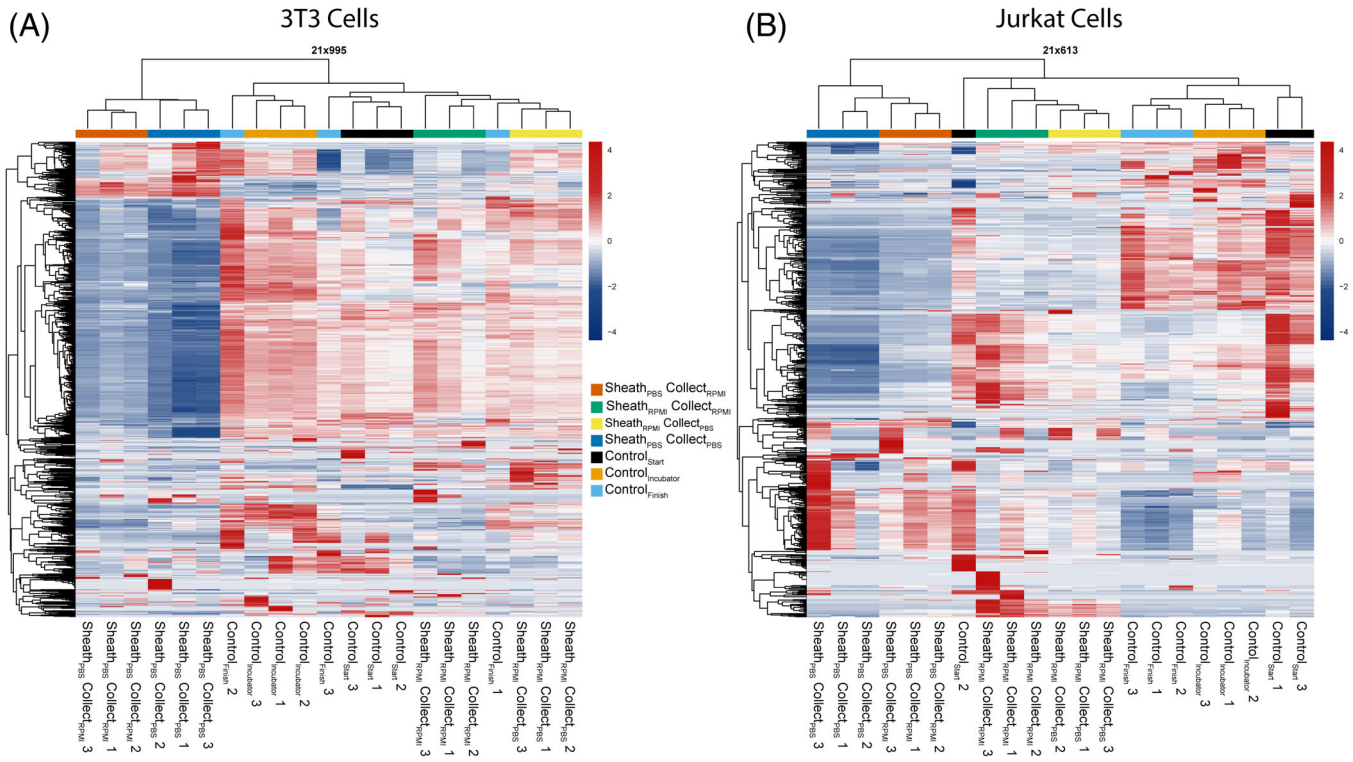

FIGURE 3 Metabolomics hierarchical clustering analysis of SICS conditions hierarchical clustering analysis of the metabolic profiles of an (A) adherent NIH/3T3 (3T3) and (B) nonadherent (Jurkat) cell. Each flow cytometry sort was carried out in technical triplicate. All replicates were derived from the same flask of cells. Color map indicates Z-score of Log2Fold change

Control$_{Incubator}$ samples were aliquoted the same was assorted cells and kept in the incubator for the duration of the experiment (*Cell Sorting and Unsorted Controls—Methods*). Cells from Sheath$_{RPMI}$ showed a very broad ($n = 431$) and asymmetric recovery of metabolite levels ($p < 0.01$, >twofold) when compared with Sheath$_{PBS}$ sorted cells (Figure 4A). Again, only a few ($n = 8$) metabolites and metabolite feature trended in the opposite direction including; AMP, IMP, Palmitoyl carnitine, and several metabolite features. These trends were also true for the Jurkat cells (Figure S4B), but the specific markers trending in the opposite direction were unique to this cell line, possibly suggesting cell-type specific stress response. Interestingly, while Sheath$_{RPMI}$ Collect$_{PBS}$ sorted cells aligned with unsorted Control$_{Start}$ samples in the first principal components (PC1), the second principal component seems to resolve samples by experimental timing (Figure 2A). The Control$_{Start}$ samples all show negative PC2 values while the unsorted Control$_{Incubator}$ (orange) cluster tightly with positive PC2 values. Further, the Control$_{Finish}$ group which was left out at room temperature shows the widest within-group variation and spans the range of PC2 values across the PCA model (sky blue). Here, the collection fluid seems to play an important role in mediating these time-dependent artifacts. We observed that Collect$_{RPMI}$ samples (green and vermillion) aligned with Control$_{Start}$ cells in the PC2 dimension while Collect$_{PBS}$ samples (yellow and blue) show more within-group variation and mostly have positive PC2 values. Finally, Sheath$_{RPMI}$ Collect$_{RPMI}$ (green) are overlapping with the Control$_{Start}$ samples in the PCA model and hierarchical clustering analysis (Figure 3), suggesting that the overall metabolic profile between these sorted cells is very similar to unsorted controls.

4.4 | Proposed SICS score

We iterated the experimental design of this study across independent frozen cell lines during the course of our efforts, but always had three shared experimental groups; Control$_{Start}$, Sheath$_{RPMI}$ Collect$_{RPMI}$, and Sheath$_{PBS}$ Collect$_{PBS}$. Therefore, we examined the overall consistency of SICS across these experiments. We exploited our double isotope-labeled ($^{13}C/^{15}N$) amino acid internal standard cocktail ($n = 16$) which is spiked into the metabolite extraction solution at 500 nM. This approach let us control for the extraction efficiency of these 16 amino acids and reduce instrument batch-effects in the meta-analysis. We then compared these amino acid levels in the two sorted conditions to the unsorted control, taking the average of the technical triplicates for each of the five experiments, and performed an unsupervised hierarchical clustering analysis (Figure 4). The Sheath$_{PBS}$ Collect$_{PBS}$ experiments clustered distinctly from the Sheath$_{RPMI}$ Collect$_{RPMI}$ experiments due to the steep and consistent loss of amino acids when using PBS for sheath fluid and sample collection fluid. These studies represent $n = 15$ technical replicates for each group, so we used these

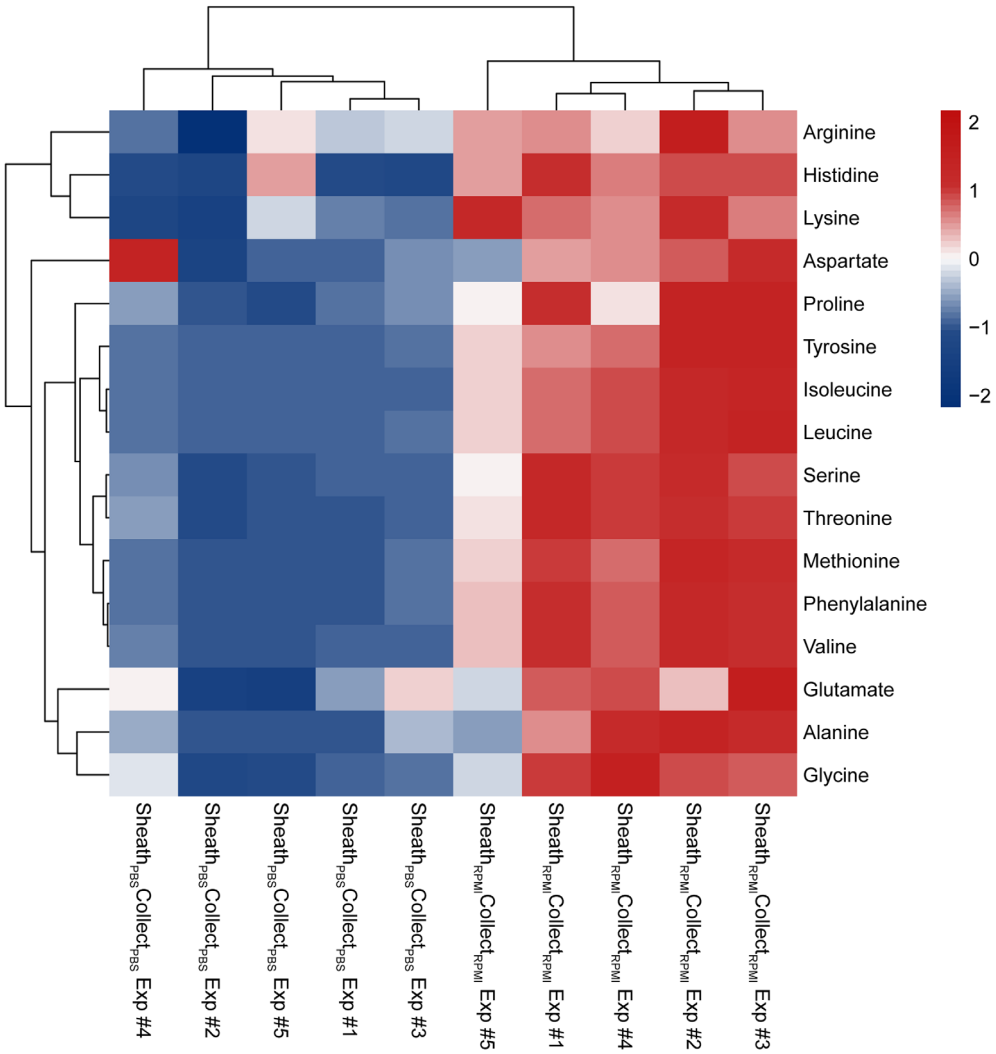

FIGURE 4 Hierarchical clustering analysis of normalized amino acids across studies hierarchical clustering analysis of select amino acids across five independent sorting experiments. Each column represents the average of technical triplicates ($n = 3$) for a single batch. Total of $n = 15$ technical replicates per group represented. Endogenous amino acids were normalized to doubly-labeled isotopic internal standards ($^{13}C/^{15}N$) spiked-in during the metabolite extraction to control for variations in extraction efficiency and instrument response over time. Each sorting condition shown (Sheath$_{PBS}$ Collect$_{PBS}$ & Sheath$_{RPMI}$ Collect$_{RPMI}$) was also taken as the ratio to the unsorted control replicates from the respective experiment. Color map indicates Z-score of Log2Fold change. Exp#5 used a PBS wash step for all samples post sort. Exp#4 represents NIH/3T3 cells

data to propose a metric for assessing the degree of SICS in a given system (Table S5). Comparing the levels of these amino acids in sorted versus unsorted controls, we take the absolute value of the median fold change (sorted/unsorted). With this metric, unsorted controls have a score of "1," while our Sheath$_{PBS}$ Collect$_{PBS}$ had a score of 8.1, and our Sheath$_{RPMI}$ Collect$_{RPMI}$ had a score of 1.1 indicating nearly complete rescue. Here, SICS = 8.1 indicates that Sheath$_{PBS}$ Collect$_{PBS}$ had 8-fold lower levels of amino acids compared with unsorted controls.

5 | DISCUSSION

Our results show that changing the sheath fluid composition and the collection fluid composition can dramatically alter the metabolites that are retained by cells with a droplet sorter. Sheath fluid and collection fluid have different effects on the profiles with sheath fluid modifying the stress on the cells while collection fluid modifies the cellular response to the stress of being sorted. Changing the sheath fluid composition likely alters the physical mechanism underlying SICS. We recognize that the time for interactions between sheath fluid and the cellular suspension is negligible during the process of cell sorting. Most droplet cell sorters have a hydrodynamically-focused laminar flow configuration which maintains a liquid–liquid boundary between sheath fluid and sample fluid until sorted cells are deposited into the collection tube and mix in a turbulent fashion. Therefore, it is surprising that changes to the sheath fluid could affect the cellular metabolic profile unless the effects are caused by sheath fluid interacting with the cells post-sort. However, our controlled comparisons with Collect$_{RPMI}$ or Collect$_{PBS}$ showed that having cell culture media in the cellular environment post-sort only partially rescues the metabolite profile, and therefore SICS likely has a major component somehow arising from the physical forces applied to cells during the sort (rapid pressure changes, high voltage potential applied, etc.). We used complete RPMI media as sheath fluid in this study, and this fluid has different physical properties than PBS. In addition to having a much more complex composition, the glucose, protein, and lipid content changes the viscosity, surface tension, buffer capacity, electrical capacitance, permittivity (dielectric), and other physicochemical properties. Any one of these factors may protect from the physical stress that results in sorter-induced cell stress (SICS).

5.1 | Sorter induced effects

For adherent NIH/3T3 cells, the use of complete media as both the sheath fluid and collection fluid seem to almost completely mitigate the markers of SICS, as well as the time-dependent experimental artifacts (PC2 discrimination, Figure 2A). Our suspension cells (Jurkat) showed the same trends (Figure 2B), indicating that SICS is a broadly observed phenomenon independent of cell type. Together, these data suggest that complete media is playing a dual role during sorting; by (a) mitigating the disruptive forces during droplet sorting, through a still uncharacterized mechanism, and by (b) maintaining the extracellular environment while cells are outside homeostatic conditions post-sort. Given the fleeting time that cells spend traveling from nozzle to collection tube (13 ms, on the SY3200 with 100 μm nozzle at 25 psi, Cytomation CytoCalc v3.2), and the short experimental duration from pre-sort cell population leading to the flash-frozen sorted-cell pellet (∼18 min), the broad loss of metabolite signals is not likely to be caused by actual differences in cellular metabolism. We incorporated a PBS wash step during the cell pelleting protocol for some replicates (Jurkat cells Exp#5) before metabolomics analysis (even for $Collect_{PBS}$ samples) and therefore our metabolite profiles reflect intracellular metabolite levels, not media contamination. However, it is not possible to fully isolate sheath and collection fluid since they mix together during collection.

5.2 | Proposed SICS model

The most likely explanation for metabolite depletion is that cytosol is being acutely lost to the surrounding fluid while traveling through the sorter. Transient membrane permeability to low molecular weight compounds (metabolites) might be caused by rapid pressurization/depressurization cycles, or by an electroporation-like effect from the high voltage pulses (positive and negative) applied to the sheath/sample fluid to charge the droplets for collection. A given cell may experience ∼15 voltage cycles before being separated into droplets at these sort rates and cell concentrations. Our latest studies are focusing on voltage and pressure effects in order to characterize the process underlying SICS in the conventional droplet cell sorter. We further examined the metabolome data to determine if there was any specificity to the metabolites lost during SICS. Using the subset of metabolites that were significantly and dramatically downregulated in $Sheath_{PBS}$ $Collect_{PBS}$ conditions compared with unsorted cells, there was actually no difference in the distribution of metabolite masses observed (Figure S5). These results support a model with broad and non-specific loss of all cellular metabolites during droplet cell sorting, and compounds at least as massive as 800–900 Da are lost without preference.

5.3 | Future directions

One major limitation of the current study is that we have yet to determine whether our observed changes in the metabolic profile can lead to the various functional deficits that have been attributed to SICS [2, 3, 11, 12]. Instead, we aimed to use metabolites as a convenient proxy of the rapid changes in the cellular state during sorting. The consistent signals that we found for SICS (e.g., nucleotide monophosphates, acyl carnitines) suggests that metabolism may indeed play a functional role in such functional deficits, at least in some cell types and situations. Whether the post-sort metabolic SICS phenotype can give rise to functional changes will be the subject of future studies, but it is clear from this report, and others, that cells sorted using droplet sorting techniques are unfit for metabolomics studies, and that the use of complete media as sheath fluid provides a way to rescue metabolic profiles similar to that of unsorted material. Another limitation is that our study utilized just one manufacturer's cell sorter, though previous reports show that SICS has been widely observed with various conventional droplet cell sorters from multiple manufacturers [2, 3, 11, 12]. Further, the potential disruptive forces discussed here are common to all droplet sorters. Although the underlying mechanism of sorter-induced cell stress remains unclear, and will be investigated in future work, the current data inform the design of such mechanistic studies, utilizing metabolomic analysis as the appropriate readout. A systematic evaluation of the effects of pressure change, nozzle-orifice size, temperature change, electrical charge, shear, acceleration, and other factors associated with droplet sorting will characterize the SICS mechanism, and point a path toward instrument modifications or practical changes to provide higher-quality sorted cells for functional assays and down-stream measurements.

ACKNOWLEDGMENTS

We are grateful to the NYULH Division of Advanced Research Technologies for supporting the core laboratories. We thank James Alvarado for aid with laboratory support. Additional thanks to Jones lab members for helpful discussion and laboratory support. Specifically, we would like to thank Yik Siu for help generating the hierarchical clustering results for the SICS score. This work was presented in part at the CYTO Virtual 2020 conference, August 4, 2020, and at the ABRF 2021 Virtual Annual Meeting, March 8, 2021.

AUTHOR CONTRIBUTIONS

Kamilah Ryan: Conceptualization; data curation; formal analysis; investigation; methodology; project administration; supervision; visualization; writing-original draft; writing-review & editing. **Rebecca Rose:** Conceptualization; data curation; formal analysis; investigation; methodology; project administration; supervision; visualization; writing-original draft; writing-review & editing. **Drew Jones:** Conceptualization; data curation; formal analysis; investigation; methodology; project administration; supervision; visualization; writing-original draft; writing-review & editing. **Peter A. Lopez:** Conceptualization; data curation; formal analysis; investigation; methodology; project administration; supervision; visualization; writing-original draft; writing-review & editing.

CONFLICT OF INTEREST

The authors declare that there is no conflict of interest.

ORCID

Peter A. Lopez https://orcid.org/0000-0002-8587-7148

REFERENCES

1. Fulwyler MJ. Electronic separation of biological cells by volume. Science. 1965;150:910–1. https://doi.org/10.1126/science.150.3698.910.
2. Bonner WA, Hulett HR, Sweet RG, Herzenberg LA. Fluorescence activated cell sorting. Rev Sci Instrum. 1972;43:404–9.
3. Andrä I, Ulrich H, Dürr S, Soll D, Henkel L, Angerpointner C, et al. An evaluation of T-cell functionality after flow cytometry sorting revealed p38 MAPK activation. Cytometry. 2020;97:171–83. https://doi.org/10.1002/cyto.a.23964.
4. Nicole White A, Janssen E, Babcock G, Worth CA, Thornton S. Different sorts for different folks: the importance of technological diversity in a cell sorting facility. J Biomol Tech. 2013;24(Suppl):S46–7.
5. Varma S, Fendyur A, Box A, Voldman J. Multiplexed cell-based sensors for assessing the impact of engineered systems and methods on cell health. Anal Chem. 2017;89:4663–70. https://doi.org/10.1021/acs.analchem.7b00256.
6. DeLay M, Lopez P, Scheinmann M "Cell Sorting for Function and Viability" CYTO 2018, 2018 Prague, Czech Republic
7. Pfister G, Toor SM, Sasidharan Nair V, Elkord E. An evaluation of sorter induced cell stress (SICS) on peripheral blood mononuclear cells (PBMCs) after different sort conditions - are your sorted cells getting SICS? J Immunol Methods. 2020;487:112902. https://doi.org/10.1016/j.jim.2020.112902.
8. Richardson GM, Lannigan J, Macara IG. Does FACS perturb gene expression? Cytometry A. 2015;87:166–75. https://doi.org/10.1002/cyto.a.22608.
9. Box A, DeLay M, Tighe S, Chittur SV, Bergeron A, Cochran M, et al. Evaluating the effects of cell sorting on gene Expression. J Biomol Tech. 2020;31:100–11.
10. Beliakova-Bethell N, Massanella M, White C, Lada S, Du P, Vaida F, et al. The effect of cell subset isolation method on gene expression in leukocytes. Cytometry A. 2014;85:94–104.
11. Sack U, Bitar M. An eloquent proof for a common challenge. Cytometry A. 2020;97A:168–70. https://doi.org/10.1002/cyto.a.23958.
12. Vidigal J, Dias MM, Fernandes F, Patrone M, Bispo C, Andrade C, et al. A cell sorting protocol for selecting high-producing subpopulations of Sf9 and high five™ cells. J Biotechnol. 2013;168:436–9. https://doi.org/10.1016/j.jbiotec.2013.10.020.
13. Llufrio EM, Wang L, Naser FJ, Patti GJ. Sorting cells alters their redox state and cellular metabolome. Redox Biol. 2018;16:381–7. https://doi.org/10.1016/j.redox.2018.03.004.
14. Binek A, Rojo D, Godzien J, Ruperez FJ, Nunez V, Jorge I, et al. Flow cytometry has a significant impact on the cellular metabolome. J Proteome Res. 2019;18:169–81. https://doi.org/10.1021/acs.jproteome.8b00472.
15. Labroots (2015) Peter Lopez - Centrifugal Elutriation - Utility in the Flow Cytometry Laboratory [Video] YouTube https://youtu.be/H5jYK8bFMek
16. Pacold ME, Brimacombe KR, Chan SH, Rohde JM, Lewis CA, Swier LJYM, et al. A PHGDH inhibitor reveals coordination of serine synthesis and one-carbon unit fate. Nat Chem Biol. 2016;12:452–8.
17. Simón-Manso Y, Lowenthal MS, Kilpatrick LE, Sampson ML, Telu KH, Rudnick PA, et al. Metabolite profiling of a NIST standard reference material for human plasma (SRM 1950): GC-MS, LC-MS, NMR, and clinical laboratory analyses, libraries, and web-based resources. Anal Chem. 2013;85:11725–31. https://www.ncbi.nlm.nih.gov/pubmed/24147600.
18. Smith CA, O'Maille G, Want EJ, Qin C, Trauger SA, Brandon TR, et al. METLIN: a metabolite mass spectral database. Ther Drug Monit. 2005;27:747–51. https://www.ncbi.nlm.nih.gov/pubmed/16404815.
19. Jones E, Oliphant E, Peterson P SciPy: Open Source Scientific Tools for Python, 2001, [cited 2019 Aug 19] http://www.scipy.org/
20. Kolde R: pheatmap: Pretty Heatmaps 2015. R package version 1.0.8 https://CRAN.R-project.org/package=pheatmap

SUPPORTING INFORMATION

Additional supporting information may be found online in the Supporting Information section at the end of this article.

How to cite this article: Ryan K, Rose RE, Jones DR, Lopez PA. Sheath fluid impacts the depletion of cellular metabolites in cells afflicted by sorting induced cellular stress (SICS). Cytometry. 2021;99:921–929. https://doi.org/10.1002/cyto.a.24361